Photostable orange-red fluorescent unsymmetrical diketopyrrolopyrrole–BF 2 hybrids

David Young, Mariusz Tasior, Adele D. Laurent, Łukasz Dobrzycki, Michal Cyrański, Nikolai Tkachenko, Denis Jacquemin, Daniel Gryko

ARTICLE

Photostable Orange-Red Fluorescent Unsymmetrical Diketopyrrolopyrrole-BF_2 Hybrids

Received 00th January 20xx,
Accepted 00th January 20xx

DOI: 10.1039/x0xx00000x

David C. Young,[a] Mariusz Tasior,[a] Adèle D. Laurent,[b] Łukasz Dobrzycki,[c] Michał K. Cyrański,*[c] Nikolai Tkachenko,*[d] Denis Jacquemin,*[b] Daniel T. Gryko*[a]

The straightforward synthesis of structurally unique DPP-BODIPY hybrids has been developed using unsymmetrical, imidazopyridine substituted DPPs. These hybrids exhibit a superb combination of photophysical properties including high photostability, good fluorescence quantum yield as well as markedly bathochromically shifted absorption and emission compared to conventional diketopyrrolopyrroles. Increasing the size of the imidazopyridine substituent and/or the electron donating power of the other aryl substituent can further redshift both absorption and emission to reach ~650 nm for the free-base and ca. 700 nm for boron-chelates. A strong intramolecular hydrogen bond is responsible for the small change in geometry between the ground and excited states and hence relatively small differences in photophysical properties upon formation of boron-chelates are observed. The solvent dependence of the photophysical properties for the free base and DPP-BF_2 complexes were investigated and show strong fluorescence with long lifetimes in both non-polar and polar aprotic environments.

Introduction

Photoluminescent organic molecules have been widely investigated for a range of applications including tunable laser dyes,[1] harvesting solar energy,[2,3] and fluorescence imaging.[4,5] Within these fields, both diketopyrrolopyrrole (DPP)[6,7] and boron-dipyrromethene (BODIPY)[8,9] based chromophores have become ubiquitous due to their favorable optical properties including large absorption coefficients, large fluorescence quantum yields and good photostability. The absorption and emission of these dyes is, however, usually localized in the green region of the visible spectrum, limiting potential biological applications. Biological imaging in the the near IR window (650-900 nm) has significant advantages over other spectral ranges due to increased tissue penetration depths, a higher signal to noise ratio and less energetic excitation wavelengths.[10-14] The use of less energetic light also extends the life of the dye, resulting in longer imaging time. Common methods used to bathochromically shift the absorption and emission of dyes, including DPPs and BODIPYs, are π-expansion, usually through planarization or annulation,[15,16] and the introduction of push-pull substituents.[17]

The combination of two or more conventional fluorophores into a single hybrid structure is a powerful method used to tune important photophysical properties of the resultant dye.[18-22] These include modulation of the absorption and emission wavelengths, Stokes shift, solvatochromism and sensory behaviour. Despite the prevalence of both BODIPYs and DPPs within the field of functional organic dyes, there have been no previous reports of a DPP core directly bonded to a difluoronated boron centre. This is undoubtedly related to the non-trivial synthesis of DPPs containing a basic nitrogen atom capable of forming a 6-membered chelate ring with a core nitrogen atom and boron atom. This problem stems from the fact that DPPs are formed in small yields or not at all from sterically bulky nitriles such as *o*-substituted benzonitriles or 1-cyanonaphthalene.[23-28] Although this problem has been apparently circumvented by others through the $POCl_3$ activated reaction of the keto group in DPP with 2-cyanomethylheterocycles or 2-aminoheterocycles to form cyanine type dyes followed by reaction with BF_3•OEt_2 (Figure 1a),[29-36] or direct reaction of a 2-pyridyl substituted DPP with BPh_3 (Figure 1b);[37] in these cases either the DPP chromophore is not preserved due to reaction of the keto groups, or a less stable non BODIPY-like 5-membered boron chelate is present. In all examples except one,[34] these reactions have been used to generate centrosymmetric dyes and a significant bathochromic shift in absorption and emission upon complexation of boron was noted. For the former case, a ca. 25 nm shift is observed moving from the free base to the di-BF_2 complex or 100 nm shift for the di-BPh_2 complex.

In this work, we establish a method for the synthesis of DPP-BF_2 hybrids, which, until now, have not yet been reported (Figure 1c). In these dyes the DPP core can be thought of as part of the dipyrrin unit which binds BF_2 in a classical BODIPY dye. These compounds were designed as a way to combine the

[a] Institute of Organic Chemistry, Polish Academy of Sciences, Kasprzaka 44–52, 01-224, Warsaw, Poland. E-mail: dtgryko@icho.edu.pl
[b] Université de Nantes, CNRS, CEISAM UMR 6230, F-44000 Nantes, France. E-mail: denis.jacquemin@univ-nantes.fr
[c] Faculty of Chemistry, University of Warsaw, Pasteura 1, 02-093 Warsaw, Poland. E-mail: mkc@chem.uw.edu.pl
[d] Chemistry and Advanced Materials Group, Faculty of Engineering and Natural Sciences, Tampere University, Korkeakoulunkatu 8, FI-33720 Tampere, Finland. E-mail: nikolai.tkachenko@tuni.fi

Electronic Supplementary Information (ESI) available: Details of syntheses; NMR, UV/vis and fluorescence spectra; fluorescence lifetime measurements; and computational computational details. CCDC 1983938. See DOI: 10.1039/x0xx00000x

beneficial features of BODIPY and DPP dyes, while downplaying their limitations. Shared attractive features of these dyes include large absorption coefficients, strong emission and high quantum yields. BODIPYs are, however, known to have very small Stokes shifts which greatly affects their detection sensitivity when used as bioimaging probes,[38] yet hybridization with other π-systems can circumvent this limitation.[16,21]

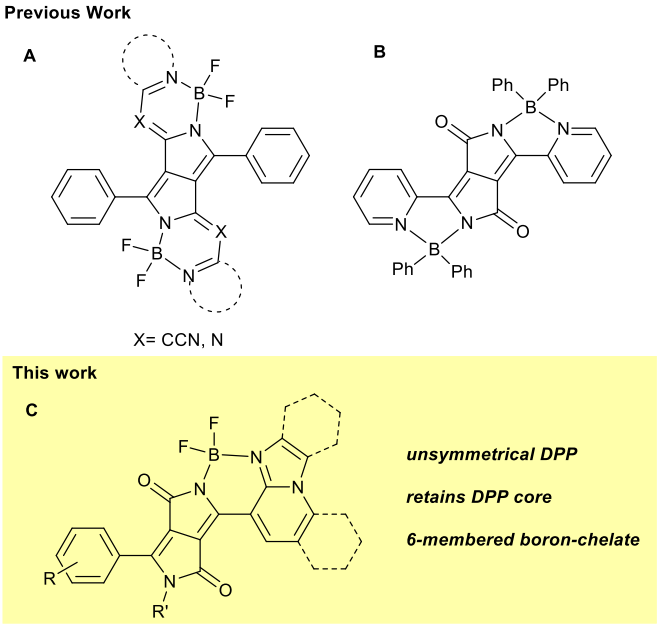

Figure 1. DPP-like and DPP chromophores containing boron.

DPP derivatives on the other hand are notoriously insoluble, as evidenced by their widespread adoption as pigments, but this can be mitigated *via* reaction of a core nitrogen atom which prevents strong intermolecular hydrogen bonding interactions. Recently, our group reported the first high yielding procedure for the regiochemical synthesis of unsymmetrical DPP derivatives through the reaction of an appropriately substituted 2-pyrrolidone with an aryl nitrile.[39] This reaction was observed to display a better tolerance for sterically bulky nitriles compared to conventional methods. Furthermore, this method additionally provides selective mono-alkylation, with the free NH being adjacent to the aryl nitrile. With this in mind, an aryl nitrile containing a Lewis base in the *ortho*- position was designed. Many potential examples fitting this criteria can be imagined, such as 8-cyanoquinolines, 4-cyanobenzimidazoles, 4-cyanobenzoxazoles, etc., however, 8-cyanoimidazo[1,2-*a*]pyridines were selected for their superb photophysical properties and relative ease of synthesis.[40-42] A strategy for the synthesis of DPP-BF_2 hybrids was therefore devised consisting of two stages: (1) the synthesis of DPPs containing a Lewis base able to form a six-membered chelate ring with the free amide nitrogen atom of the DPP core, and (2) the coordination of the boron centre using analogous conditions used to make BODIPY from dipyrrins.

The photophysical properties of the free base DPPs and their respective DPP-BF_2 hybrids were investigated in a variety of solvents and rationalized using computational methods.

Results and discussion

Design and synthesis

Six heterocyclic imidazopyridines containing an appropriately placed nitrile functional group were synthesized which differed by either appended functional group or extent of the fused π-system. The size of these heterocycles ranged from small imidazo[1,2-*a*]pyridine derivatives through imidazo[1,2-*a*]quinoline and benzo[*b*]imidazo[1,2-*a*]quinoline to dibenzo[*b*,*f*][4,5]imidazo[1,2-*a*]quinoline (Table 1, **2a**-**2f**).

The imidazo[1,2-*a*]pyridine-derived nitriles **2a**-**2c**, were synthesized *via* the condensation of 2-aminonicotinonitrile with either chloroacetaldehyde[43] or appropriate α-bromoketones according to literature procedures.[44] Nitrile **2d** was synthesized from 2-amino-3-cyanoquinoline[45] using a method analogous to that described for **2a**. Nitriles **2e** and **2f** were synthesized from (2-benzimidazolyl)acetonitrile and either 2-chlorobenzaldehyde or 1-bromo-2-naphthaldehyde *via* a thermally induced cyclization step in sulfolane according to a literature procedure.[46]

The reasoning behind the design and synthesis of imidazo[1,2-a]pyridine derivatives with increasingly large π-systems is that this is expected to bathochromically shift the absorption and emission spectra of the resultant compounds increasing their potential utility for biological applications.

The second aryl substituent on the DPP core (derived from pyrrolidone **1**) was chosen based on the photophysical characteristics of previously reported unsymmetrically substituted diketopyrrolopyrroles.[39] In particular, it was found that a 4-methoxyphenyl substituent makes DPPs fluorescence independent on solvent polarity, whereas the 4-dimethylaminophenyl substituent shifts emission bathochromically and induces strong solvatofluorochromism. A 2-methoxyphenyl substituent was also selected as an electrically similar substituent, yet it has significantly different geometrical properties due to the increased steric profile of the *ortho*-substituent.

All six imidazo[1,2-*a*]pyridine derivatives **2a**-**2f** were reacted with an appropriate 2-pyrrolidone (**1a**-**1c**) to give unsymmetrical DPP derivatives **3a**-**3i** capable of forming six-membered chelate rings with Lewis acids (Table 1). The yields of this reaction are moderate, and generally decrease with the size of the aryl nitrile. In particular, the yield of **3f**, containing the largest substituent, is lower than the others, which is attributed to the solubility of this nitrile in the reaction conditions. It is important to note that this represents the largest aromatic nitrile to be incorporated directly into a DPP core. The substituent on the 2-pyrrolidone ring was not observed to influence the yield of the DPP substantially.

Having DPPs **3a**-**3f** in hand, the stage was set to start their complexation with boron. A difluoro-bora unit was selected as the chelating motif due to its ubiquity in dye chemistry and beneficial photophysical properties. The synthesis of these complexes was achieved in a one-pot procedure involving the deprotonation of the DPP with base in dichloromethane followed by treatment with boron trifluoride etherate. This resulted in compounds **4a**-**4i** in initially moderate to low yields

(Table 1). The yield of **3f** precluded attempts at the synthesis of its BF_2 hybrid analogue. A point of difference to conventional BODIPY dyes is that one of the nitrogen donors is in the form of a lactam, rather than the more commonly reported pyrrole. The presence of this functional group is thought to be responsible for the lower yields compared to those typically reported for BODIPY syntheses using tertiary amines as the base,[47-50] possibly due to interaction of BF_3 with the amide oxygen atom. Boron complexes containing a nitrogen donor that is part of a cyclic amide functional group have been reported previously and have features such as large Stokes shifts, high quantum yields, and long absorption and emission wavelengths.[51] In these cases, low to moderate synthetic yields were also reported.[52-54] In order to optimize this reaction, LiHMDS was trialled as a base based on a previous study[55] and higher yields were observed.

Table 1. Synthesis of nnsymmetrical DPPs and BF_2-DPP Hybrids.

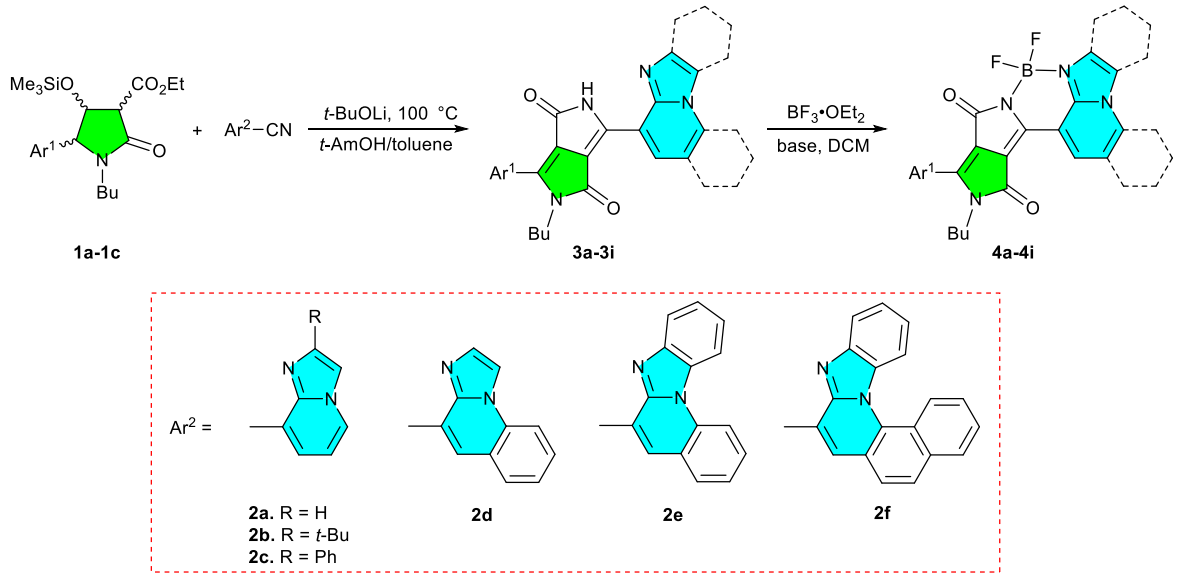

Pyrrolidone	Ar_1	Ar_2	DPP	Yield [%]	Base	BF_2-DPP	Yield [%]
1a	4-methoxyphenyl	**2a**	**3a**	61	LiHMDS/Et_3N	**4a**	37/5
1a	4-methoxyphenyl	**2b**	**3b**	45	LiHMDS	**4b**	50
1a	4-methoxyphenyl	**2c**	**3c**	59	LiHMDS	**4c**	44
1a	4-methoxyphenyl	**2d**	**3d**	50	LiHMDS	**4d**	46
1a	4-methoxyphenyl	**2e**	**3e**	53	LiHMDS/Et_3N	**4e**	62/9
1a	4-methoxyphenyl	**2f**	**3f**	11	LiHMDS	**4f**	N/A
1b	2-methoxyphenyl	**2a**	**3g**	33	Et_3N	**4g**	5
1b	2-methoxyphenyl	**2e**	**3h**	48	LiHMDS/Et_3N	**4h**	41/9
1c	4-(dimethylamino)phenyl	**2e**	**3i**	57	Et_3N	**4i**	10

Photophysical Properties

The photophysical properties of the free base DPPs and their respective DPP-BF_2 hybrids were investigated in a variety of solvents. Absorption and emission data for compounds **3a**-**3i** and **4a**-**4i** in $CHCl_3$ are presented in Table 2 (for other solvents, see Table S1).

For the free base DPPs, two vibronic absorption maxima are evident in the visible region in all cases, separated by 35-41 nm. The molar absorption coefficients for these bands are in the range 15000-27100 $M^{-1}cm^{-1}$, consistent with other DPP derivatives.[56] While the two maxima have similar intensities, the redder band is more intense for dyes **3a**-**3d**, which contain smaller aryl substituents, whereas the bluer is stronger for dyes **3e** and **3f**, which contain larger π-systems. Expansion of the imidazopyridyl substituent red-shifts the absorption maxima by 10-21 nm per additional benzannulation (Figure 2a). A negligible shift in maxima is observed for **3a**-**3c**, indicating the chosen substituents of the imidazo[1,2-*a*]pyridine ring do not significantly contribute to the excitation process.

The effect the second electron-rich aryl substituent has on the absorption properties of the free base DPPs turns out to be quite significant (Figure 2b). Whereas the two absorption bands of **3e**, which contains a 4-methoxyphenyl substituent, are approximately equal, upon moving to a 2-methoxy substituent the higher energy band strongly dominates and both bands are hypsochromically shifted by circa 10 nm.

Replacement of the 4-methoxyphenyl substituent with the more strongly donating 4-dimethylaminophenyl substituent has the opposite effect on the band intensities, and the redder absorption band dominates. The positions of the peaks are also dramatically red-shifted by ca. 30 nm, in accordance with a previous study on structurally simpler, unsymmetrical DPPs possessing a single 4-dimethylaminophenyl group.[39]

Upon increasing the solvent polarity, a slight hypsochromic shift is observed in both absorption (Figure 2c) and emission spectra (Figures S1-S16).

Table 2. Photophysical properties of free base DPPs and DPP-BF_2 Hybrids in $CHCl_3$.

Compound	$^{max}\lambda_{abs}$ [nm]	ε_{max} [$M^{-1}cm^{-1}$]	$^{max}\lambda_{ems}$ [nm]	Stokes shift [cm^{-1}]	Φ_{fl}[a]	τ_F [ns]	k_r [10^8 s^{-1}]	k_{nr} [10^8 s^{-1}]
3a	509, 544	15000, 15900	569, 614	810	0.63	5.5	1.1	0.7
3b	509, 544	17400, 18500	568, 613	780	0.61	5.2	1.2	0.8
3c	513, 548	24100, 25400	573, 618	800	0.58	5.1	1.1	0.8
3d	517, 554	19600, 20400	581, 629	840	0.70	5.1	1.4	0.6
3e	530, 567	25100, 24700	597, 646	890	0.36	3.3	1.1	1.9
3f	547, 588	27100, 26200	618, 673	830	0.38	2.8	1.4	2.2
3g	501, 530	15600, 13800	566, 611	1200	0.50	5.5	0.9	0.9
3h	521, 555	22400, 20100	595, 640	1210	0.27	3.1	0.9	2.4
3i	557, 596	27300, 35600	636, 687	1060	0.69	4.3	1.6	0.7
4a	546	10100	608	1870	0.31	5.8	0.5	1.2
4b	534, 570	13700, 14700	606	1040	0.42	5.8	0.7	1.0
4c	537, 574	11100, 11500	611, 655	1050	0.47	5.9	0.8	0.9
4d	546, 585	16300, 16200	625	1090	0.50	5.3	0.9	0.9
4e	566, 603	22400, 21200	652	1250	0.22	3.0	0.7	2.6
4g	525, 558	15000, 13700	604, 654	1360	0.51	6.0	0.9	0.8
4h	555, 583	10700, 9200	656	1910	0.07	2.5	0.3	3.7
4i	601, 644	13300, 14400	702	1280	0.27	2.9	0.9	2.5

[a]Determined using Rhodamine 6g in EtOH.

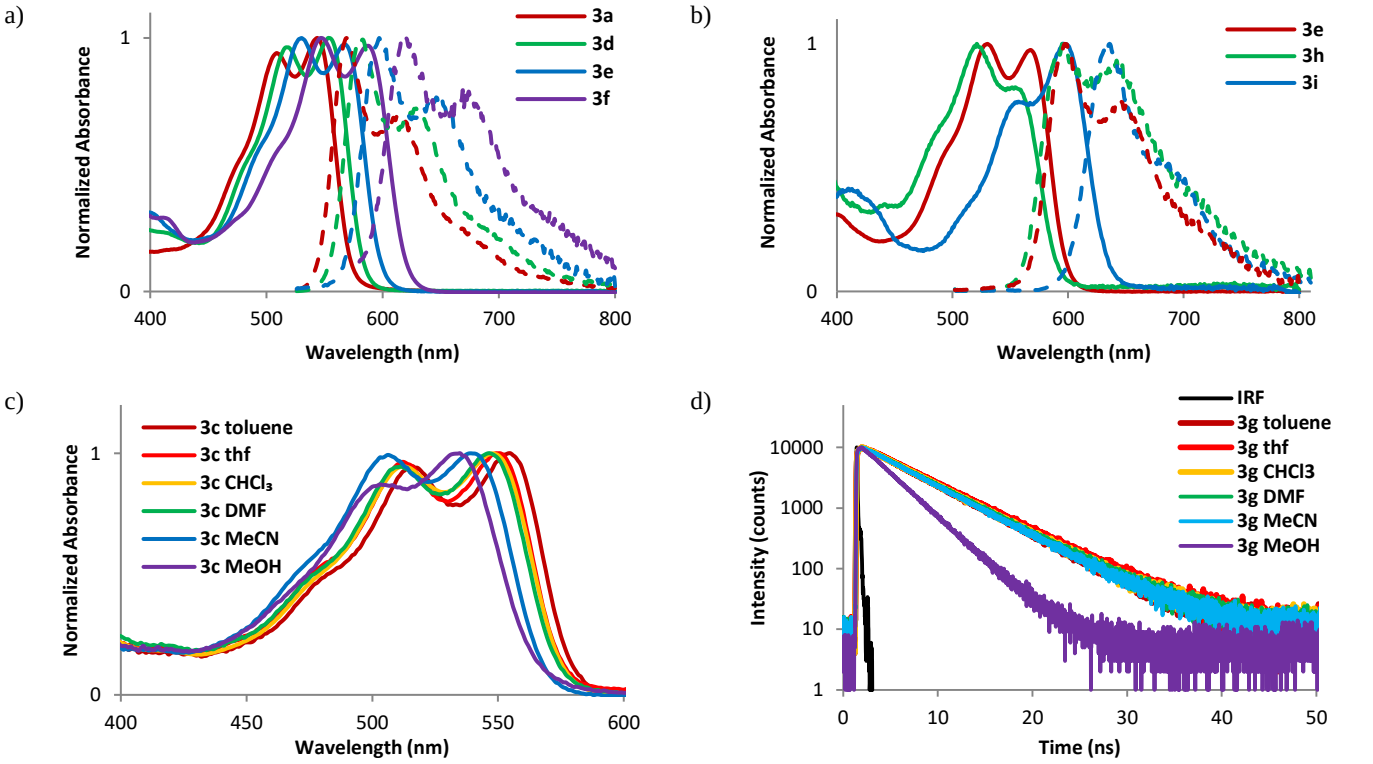

Figure 2. a) Effect of π-expansion on the absorption and emission of free base DPPs in $CHCl_3$. b) Effect of the other aryl substituent on the absorption and emission properties of DPPs in $ChCl_3$ (4-methoxyphenyl - red; 2-methoxyphenyl - green; 4-dimethylaminophenyl - blue). c) Hypsochromic solvatochromism of representative example **3c**. d) Fluorescence lifetimes of representative example **3g** in a range of solvents highlighting the drop in protic methanol (see SI for other examples).

Two emission maxima are also observed for the free base DPPs with similar separation on the energy scale to absorption indicating the involvement of vibronic coupling. The trend of increasing separation with increasing size of π-system is preserved.

The Stokes shifts are very low for DPPs (circa 800-1200 cm^{-1} in $CHCl_3$), possibly a consequence of the rigid planarity enforced by an intramolecular hydrogen bonding interaction between the core amide NH and basic nitrogen atom of the imidazopyridine substituent. This interaction is confirmed in the solid state by single crystal X-ray diffraction analysis of **3d** (Figure 3). Two dye molecules are present in the asymmetric unit, each displaying lower angles between the mean plane of the core and mean plane of the imidazopyridine substituent than the core and the 4-methoxyphenyl substituent (1.2 and 5.9° vs 7.0 and 18.7°, respectively). Disorder in the orientation of the butyl chains in both, in addition to the pyrrole skeleton in one molecule is also observed. The large, relatively flat molecules are arranged in a head-to-tail π-π stacking motif along the crystallographic b-axis with no significant interactions in any other dimensions (Figure S34).

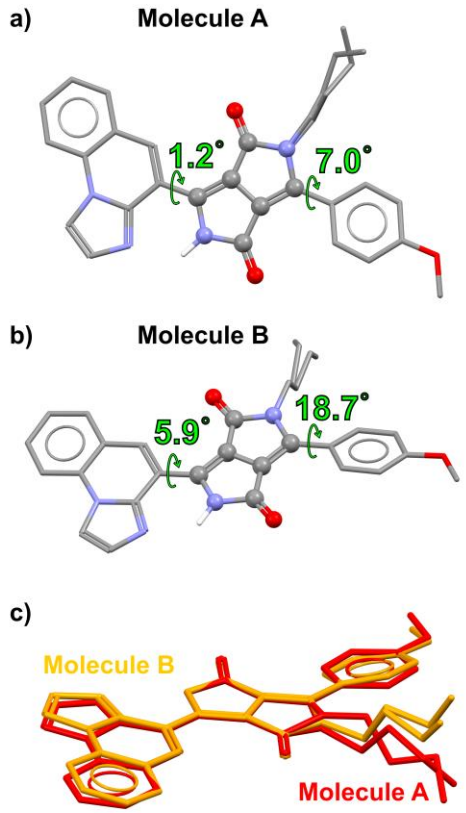

Figure 3. Single crystal X-ray structure of **3d**. Two molecules are present in the asymmetric unit (a and b) which differ by orientation of substituents (c). CH hydrogen atoms are omitted for clarity.

This intramolecular hydrogen bonding interaction, especially in non-polar solvents, is expected to enforce co-planarity between the core and substituent in both the ground and excited states. Indeed, the Stokes shift is noticeably larger in the protic solvent methanol, which is capable of disrupting this interaction. The position of these emission maxima are bathochromically shifted as the π-system is enlarged, culminating in red emission at 673 nm in $CHCl_3$ by **3f**. In an analogous trend to absorption, replacement of the 4-methoxyphenyl substituent with 2-methoxyphenyl slightly blue-shifts the emission, whereas replacement with 4-dimethylaminophenyl strongly bathochromically shifts the emission. Expanding the π-system of the imidazopyridine, while bathochromically shifting both the absorption and emission, has a negative impact on the quantum yield and fluorescent lifetime. This is a consequence of the well-known energy gap law: as the HOMO-LUMO gap decreases, the non-radiative decay pathways become more efficient.

The quantum yields and fluorescence lifetimes of **3a**-**3f** are relatively unchanged in a range of common non-polar and polar aprotic solvents, however, they are observed to decrease in methanol (representative example shown in Figure 2d, for others see SI). This is likely a consequence of the higher propensity for internal conversion to the ground state due to hydrogen bonding interactions of the solvent to polar moieties of the chromophore (e.g., MeO-H···O=CN) and the high frequency vibrational modes these create. This trend is slightly more evident in the case of the 2-methoxyphenyl substituted derivates **3g** and **3h** and extreme in the dimethylaminophenyl substituted **3i** where the quantum yield diminishes from almost unity in toluene to less than 1% in methanol.

In short, it is evident that both the imidazopyridyl and aryl substituents of the free base DPPs **3a**-**3i** are able to tune the visible absorption (503 to 602 nm) and emission (562 to 691 nm) maxima, allowing for a high level of control of the photophysical properties.

A momentous change in photophysical properties, such as moving from a simple dipyrromethene to a BODIPY dye, is not observed upon moving from **3** to **4** (Figure 4). This is likely due to the already highly conjugated and polar structure of the DPP core. In all cases the absorption and emission maxima of **4a**-**4i** are slightly red-shifted relative to their corresponding free base analogues. A broadening of the absorption and emission spectra is also observed, concurrent with larger Stokes shifts and a noticeable drop in the molar absorption coefficients and quantum yields. Broadening is particularly evident in DPP-BF_2 hybrids with larger π-systems (**4d**, **4e**) and in polar solvents (DMF, MeCN and MeOH). In some cases (**4a**, **4b**, **4d**, **4d**, **4h**, **4i**) only one emission maxima can be clearly observed, the second vibronic maxima appearing as a shoulder on the red side. These observations are likely due to increased charge transfer from the electron-rich methoxyphenyl or dimethylaminophenyl substituent to the DPP-BF_2 hybrid core and are a result of the increased reorganization energy of excitation and emission. This is an expected observation as BODIPY cores are known to act as very strong acceptors.

Although the quantum yields are lowered for the hybrids with respect to the free bases, fluorescent lifetimes remain approximately unchanged (~5 ns in aprotic solvents for **3a**/**4a**-

3d/**4d**; ~3 ns for **3e**/**4e**). This is mainly due to the lower value of the radiative rate constant (k_r in Table 2) which is directly proportional to the oscillator strength; therefore, a lower value of k_r is in agreement with the general trend of lower molar absorption of boron-chelated compounds, as noted above.

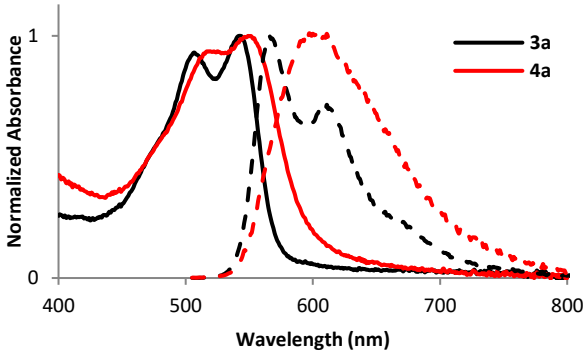

Figure 4. Absorption and emission spectra of **3a** and **4a** in DMF.

The relative drop in fluorescence lifetime of DPP-BF_2 hybrids in methanol compared to other solvents is less evident than for free base DPPs. Protection of the amide-like nitrogen atom of the DPP core may be responsible for this as hydrogen bonding interactions contributing to non-radiative decay pathways are lessoned.

Spectral Fitting

To a first approximation, absorption and emission spectra can be represented by a superposition of Gaussian bands; each of which represent a transition from the ground vibrational level of the initial electronic state (ground state for absorption and excited state for fluorescence) to one of the vibrational levels of the product (electronically excited state and ground state for absorption and emission, respectively). The two closest bands in the absorption and emission spectra are transitions from one "zero" vibrational level to another "zero" vibrational level, thus the name E_{00}. The shift between these two bands, also known as Stokes shift, is determined by the reorganization energy, E_{reorg}, and is roughly equal to $2E_{reorg}$. The contribution of transitions to different vibrational levels is determined by the Franck-Condon factor and was evaluated and applied by Marcus to the so-called inverted regime of electron transfer,[57] but the theory can also be applied to analyze absorption and emission spectra of dyes.[58-60] The functional wavelengths for absorption, $A(\lambda)$, and emission spectra, $I(\lambda)$, are given by the equations:

$$A(\lambda) = A_0 \sum_{i=0}^{\infty} \frac{S^i}{i!} exp\left[-\frac{\left(\Delta G + E_{out} + ihv_{vib} - \frac{hc}{\lambda}\right)^2}{2E_{out}k_BT} \right] \quad (1)$$

$$I(\lambda) = \frac{B_0}{\lambda^5} \sum_{i=0}^{\infty} \frac{S^i}{i!} exp\left[-\frac{\left(\Delta G - E_{out} - ihv_{vib} - \frac{hc}{\lambda}\right)^2}{2E_{out}k_BT} \right] \quad (2)$$

where $\Delta G = -E_{00}$ is the free energy or the energy difference between electronic ground and excited states, E_{out} is the outer sphere reorganization energy, also known as the solvent reorganization energy, hv_{vib} is the vibration mode energy, and S is the so called electronic-vibrational coupling which is associated with internal reorganization energy, E_{in}, as $S = E_{in} / hv_{vib}$.

These equations were used to simultaneously fit the absorption and emission spectra for selected compounds in chloroform, an example of which is shown in Figure 5. Results of the fitting are presented in Table 3. The vibrational splitting is much more pronounced in the model spectra, which indicates that the reorganization energy is underestimated by the fit model. This was the case in all fits. The most accurate parameter from the fit is ΔG, with an accuracy of roughly ±0.002 eV. The energy of the vibrational mode (hv_{vib}) is virtually the same for all molecules and well within the range of many other dyes. The solvent reorganization energy (E_{out}) is relatively small for all compounds in chloroform which means that there isn't a large change in the static dipole moment on transition from the ground to singlet excited state. This usually indicates weak solvent polarity dependence, implying the vastly different photophysical properties of the dyes in the polar protic solvent are due to hydrogen bonding interactions. Interestingly, the internal reorganization energy (E_{in}) is relatively large for all compounds, though this is the least accurate parameter from the fit.

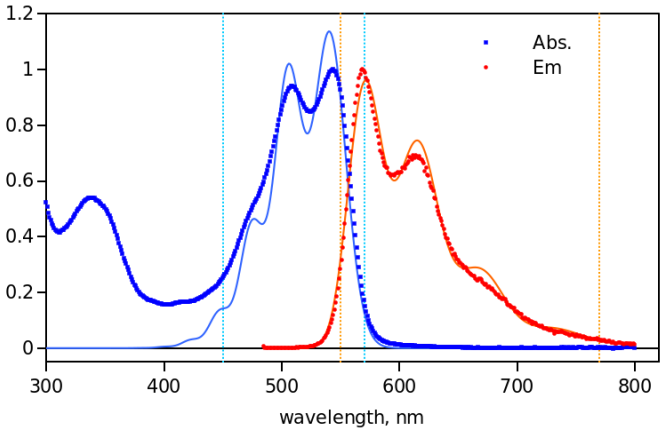

Figure 5. Absorption (blue) and emission (red) spectra of **3a** in chloroform (symbols) and corresponding fits (solid lines). Dashed vertical lines indicate the fit range limits (though the fits are drawn beyond the limits).

The table also shows the difference between the free base and BF_2 hybrids (**3** vs **4**). Presumably, the larger change in the molecular geometry upon addition of BF_2, increases the difference in ΔG values.

Table 3. Energy parameters estimated from global absorption and emission spectra fits of compounds in chloroform.

Compound	Δ*G* [eV]	E_{out} [eV]	hv_{vib} [eV]	S	E_{in} [eV]
3a	2.229	0.061	0.157	0.898	0.141
4a	2.132	0.083	0.153	0.755	0.115
3a – **4a**	0.097				0.026
3e	2.131	0.064	0.157	0.969	0.152
4e	1.987	0.081	0.153	1.005	0.154
3e – **4e**	0.144				–0.002
3h	2.158	0.077	0.158	1.122	0.177
4h	2.002	0.091	0.156	1.105	0.172
3h – **4h**	0.156				0.005
3i	2.016	0.066	0.157	0.662	0.104
4i	1.856	0.068	0.146	0.965	0.141
3i – **4i**	0.160				–0.037

Table 4. Comparison between theoretical and experimental 0-0 wavelengths

Compound	Experiment [nm]	Theory[nm]
3a	557	558
4a	577	583
3b	556	557
4b	588	579
3c	561	561
4c	593	584
3d	568	-
4d	605	-
3e	582	579
4e	628	609
3f	603	599
4f	-	630
3g	548	554
4g	581	579
3h	573	574
4h	620	606
3i	596	608
4i	673	647

Theoretical Studies

To shed more light onto the nature of the electronic processes involved in these systems, we have performed theoretical calculations using a protocol that is suited for such conjugated derivatives[61] and is detailed in the ESI.

To provide a quantitative comparison between theory and experiment, we report in Table 4 the theoretical 0-0 energies and compare them to their experimental counterparts. Indeed, we recall that such comparisons are theoretically well grounded, whereas comparing vertical transition energies to experimental λ_{abs} or λ_{ems} is a more approximated approach.[62] The agreement between theory and experiment in this case is really remarkable with a mean absolute deviation as small as 8 nm. More importantly, the trends are well described by theory, with; i) successive bathochromic shifts of ca. 10 nm per annulation when expanding the size of the imidazopyridine substituents; ii) a larger +30 nm displacement when the methoxyphenyl aryl substituent is replaced by dimethylaminophenyl (**3e** to **3i**); and iii) redshifts induced by the complexation of BF_2 (**3** to **4**). This clearly suggests that the selected level of theory is suited for the analysis of this series of compounds.

The electron density difference (EDD) plots for six representative compounds can be found in Figure 6. In all free base structures, the presence of an intramolecular hydrogen bond constrains the DPP core and imidazopyridyl substituent in a coplanar arrangement. This rigidified structure is consistent with the large quantum yields of emission. In **3a**, the excited-state is mostly localised on the DPP core and partly on the vicinal imidazopyridine moiety that is coplanar. The methoxyphenyl substituent only plays a trifling role. The transition has local π–π* character, with no significant charge transfer (CT), as measured by Le Bahers' metric[63,64] which returns the small value of 0.35 e^- over 1.27 Å. It is nevertheless interesting to note that the transition induces a small decrease of the excited-state dipole-moment (by −1.6 D), which is totally consistent with the negative solvatochromism observed experimentally.

In the corresponding difluoroborate complex, **4a**, the nature of the excited state is globally preserved, but it is slightly more delocalized. Accordingly, the CT becomes slightly larger (0.41 e^- over 2.42 Å), and the decrease of the excited-state dipole moment is slightly larger than in **3a** (−3.5 D). This increase of the CT character of the excited-state in going from **3a** to **4a** is qualitatively consistent with the experimental outcomes, that is, the broadening of the absorption spectra, the small red-shift of the absorption and emission bands upon complexation of the boron, and the larger Stokes shift of **4a** compared to **3a**.

By increasing the size of the π-conjugated moiety in **3e** and **4e**, the nature of the electronic transition is not fundamentally changed, but it becomes slightly more delocalized, especially in the difluoroborate hybrid that now undergoes a CT of 0.45 e^- over 3.01 Å, which means that the transition has a mixed local/CT character. Note that in going from **3e** to **4e**, the computed oscillator strength slightly decreases, although the molecular weight of the compound is increased, consistent with the decrease of ε values noted experimentally.

The 4-dimethylaminophenyl substituent is calculated to have an even more significant impact as it induces a larger CT

compared to the analogous methoxyphenyl substituted compounds. The calculated CT of 0.51 e^- over 3.90 Å for **4i** is consistent with the extreme red-shift observed experimentally for this compound.

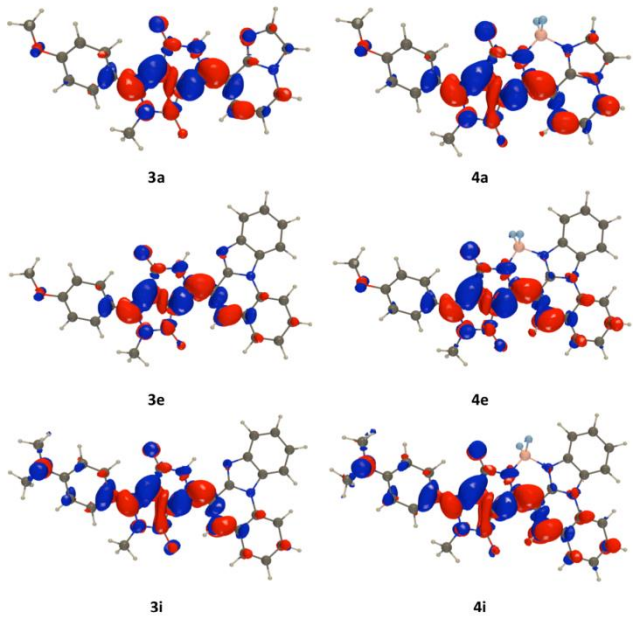

Figure 6. EDD plots for six compounds. The blue (red) regions represent regions of loss (gain) of electronic density upon photon absorption. Contour threshold: 1 x 10^{-3} au.

Photostability

The photostability of the free base DPPs and DPP-BF_2 hybrids were studied in methanol using a xenon light source (Figure 7). In all cases the DPP-BF_2 hybrids displayed greater stability than their free base analogues. In particular, DPP-BF2 compounds bearing a bulky moiety on the imidazopyridine substituent (**4b** and **4c**) displayed the greatest increase in stability. The hybrids also showed greater stability with respect to a more conventional DPP derivative and were more similar to a BODIPY derivative known for stability.

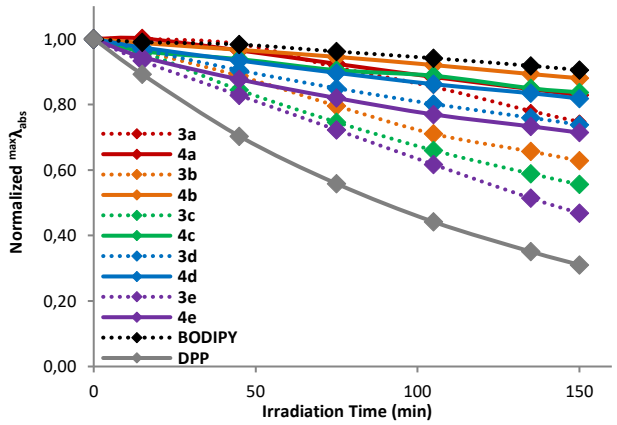

Figure 7. Photostability of DPP and DPP-BF_2 derivatives compared to a BODIPY (BODIPY 493/503) and DPP (2,5-dibutyl-3,6-bis(3,4-dimethoxyphenyl)pyrrolo[3,4-*c*]pyrrole-1,4(2*H*,5*H*)-dione) measured using a collimated light source from a 300W Xe lamp.

Conclusions

In conclusion, we have proven that DPP-BODIPY hybrids can be synthesized by taking advantage of an imidazopyridine substituent linked directly to a diketopyrrolopyrrole core. The arrangement of nitrogen atoms allows this substituent to act as a ligand for Lewis acids. This method is amenable to both small and large imidazopyridine derivatives (from 2 to 5 fused aromatic rings). The inclusion of such bulky substituents on a DPP is almost unprecedented due to previous synthetic challenges. For the first time the influence of the size of the aryl substituent directly attached to the DPP core could be studied revealing that, extension of the π-system by increasing the size of the imidazopyridine moiety shifts the absorption and emission maxima by 10-20 nm per additional benzo unit. This influence is related to the presence of an intramolecular hydrogen bond in the free-bases and the coordination bonds in boron-chelates which planarizes the conformation in the ground state. The ability to independently alter the structure of both the imidazopyridyl and the second aryl substituents enables tuning of the absorption (503 to 602 nm) and emission (562 to 691 nm) maxima, for both free base DPPs and DPP-BF_2 hybrids in a range of solvents. While the absorption and emission of the hybrids were bathochromically shifted with respect to their precursors, the free bases exhibited brighter emission. The new dyes have strong fluorescence responses in all solvents almost regardless of polarity and proticity unless a stronger donor substituent (4-dimethylaminophenyl) is present. Importantly, the photostability of the DPP-BF_2 hybrids was also found to be markedly better than conventional DPPs making them more in-line with BODIPY derivatives. Intense and almost solvent independent fluorescence combined with high photostability will allow their use in modern super resolution imaging techniques.

Conflicts of interest

There are no conflicts to declare.

Acknowledgements

The authors would like to thank the Foundation for Polish Science (TEAM POIR.04.04.00-00-3CF4/16-00) and the Global Research Laboratory Program (2014K1A1A2064569) through the National Research Foundation (NRF) funded by Ministry of Science, ICT & Future Planning (Korea). This research used resources of i) CCIPL (Centre de Calcul Intensif des Pays de Loire); ii) a local Troy cluster; and iii) HPC resources from ArronaxPlus (grant ANR-11-EQPX-0004 funded by the French National Agency for Research).

.

Notes and references

1 A. J. C. Kuehne and M. C. Gather, *Chem. Rev.*, 2016, **116**, 12823-12864.

2 L. Meng, Y. Zhang, X. Wan, C. Li, X. Zhang, Y. Wang, X. Ke, Z. Xiao, L. Ding, R. Xia, H.-L. Yip, Y. Cao and Y. Chen, *Science*, 2018, **361**, 1094-1098.

3 W. Li, K. H. Hendriks, M. M. Wienk and R. A. J. Janssen, *Acc. Chem. Res.*, 2016, **49**, 78-85.

4 L. Long, M. Huang, N. Wang, Y. Wu, K. Wang, A. Gong, Z. Zhang and J. L. Sessler, *J. Am. Chem. Soc.*, 2018, **140**, 1870-1875.

5 M. J. Schnermann, *Nature*, 2017, **551**, 176-177.

6 M. Grzybowski and D. T. Gryko, *Adv. Opt. Mater.*, 2015, **3**, 280-320.

7 M. Kaur and D. H. Choi, *Chem. Soc. Rev.*, 2015, **44**, 58-77.

8 A. Loudet and K. Burgess, *Chem. Rev.*, 2007, **107**, 4891-4932.

9 G. Ulrich, R. Ziessel and A. Harriman, *Angew. Chem. Int. Ed.*, 2008, **47**, 1184-1201.

10 J.-B. Li, H.-W. Liu, T. Fu, R. Wang, X.-B. Zhang and W. Tan, *Trends Chem.*, 2019, **1**, 224-234.

11 Q. Miao and K. Pu, *Adv. Mater.*, 2018, **30**, 1801778.

12 P. Reineck and B. C. Gibson, *Adv. Opt. Mater.*, 2017, **5**, 1600446.

13 E. A. Owens, M. Henary, G. El Fakhri and H. S. Choi, *Acc. Chem. Res.*, 2016, **49**, 1731-1740.

14 J. V. Frangioni, *Curr. Opin. Chem. Biol.*, 2003, **7**, 626-634.

15 M. Stępień, E. Gońka, M. Żyła and N. Sprutta, *Chem. Rev.*, 2017, **117**, 3479-3716.

16 H. Lu, J. Mack, Y. Yang and Z. Shen, *Chem. Soc. Rev.*, 2014, **43**, 4778-4823.

17 S. Xuan, N. Zhao, X. Ke, Z. Zhou, F. R. Fronczek, K. M. Kadish, K. M. Smith and M. G. H. Vicente, *J. Org. Chem.*, 2017, **82**, 2545-2557.

18 M. Havlík, V. Talianová, R. Kaplánek, T. Bříza, B. Dolenský, J. Králová, P. Martásek and V. Král, *Chem. Commun.*, 2019, **55**, 2696-2699.

19 K. Huang, X. Jiao, C. Liu, Q. Wang, X. Qiu, D. Zheng, S. He, L. Zhao and X. Zeng, *Dyes Pigm.*, 2017, **142**, 437-446.

20 J. Chen, W. Liu, B. Zhou, G. Niu, H. Zhang, J. Wu, Y. Wang, W. Ju and P. Wang, *J. Org. Chem.*, 2013, **78**, 6121-6130.

21 A. Y. Bochkov, I. O. Akchurin, O. A. Dyachenko and V. F. Traven, *Chem. Commun.*, 2013, **49**, 11653-11655.

22 T. Kim, W. Kim, O. Vakuliuk, D. T. Gryko and D. Kim, *J. Am. Chem. Soc.*, 2020, **142**, 1564-1573.

23 L. C. A. C. Rochat, A. Iqbal, (Ciba-Geigy Ltd.), Eur. Pat. Appl. 94911., 1983.

24 B. L. Kaul, (MCA Technologies GMBH), Int. Pat. Appl. WO2004076456, 2004.

25 H. O. H. Yamamoto, M. Duggeli, (Ciba Specialty Chemicals Holding Inc.), Int Pat. Appl. WO2006061343., 2006.

26 H. Langhals, T. Potrawa, H. Nöth and G. Linti, *Angew. Chem. Int. Ed. Engl.*, 1989, **28**, 478-480.

27 S. Luňák, L. Havel, J. Vyňuchal, P. Horáková, J. Kučerík, M. Weiter and R. Hrdina, *Dyes Pigm.*, 2010, **85**, 27-36.

28 T. Potrawa and H. Langhals, *Chem. Ber.*, 1987, **120**, 1075-1078.

29 S. Shimizu, T. Iino, A. Saeki, S. Seki and N. Kobayashi, *Chem.: Eur. J.*, 2015, **21**, 2893-2904.

30 Y. Kage, S. Mori, M. Ide, A. Saeki, H. Furuta and S. Shimizu, *Mater. Chem. Front.*, 2018, **2**, 112-120.

31 S. Shimizu, T. Iino, Y. Araki and N. Kobayashi, *Chem. Commun.*, 2013, **49**, 1621-1623.

32 S. Wiktorowski, C. Rosazza, M. J. Winterhalder, E. Daltrozzo and A. Zumbusch, *Chem. Commun.*, 2014, **50**, 4755-4758.

33 T. Marks, E. Daltrozzo and A. Zumbusch, *Chem.: Eur. J.*, 2014, **20**, 6494-6504.

34 G. M. Fischer, C. Jüngst, M. Isomäki-Krondahl, D. Gauss, H. M. Möller, E. Daltrozzo and A. Zumbusch, *Chem. Commun.*, 2010, **46**, 5289-5291.

35 G. M. Fischer, M. Isomäki-Krondahl, I. Göttker-Schnetmann, E. Daltrozzo and A. Zumbusch, *Chem.: Eur. J.*, 2009, **15**, 4857-4864.

36 G. M. Fischer, A. P. Ehlers, A. Zumbusch and E. Daltrozzo, *Angew. Chem. Int. Ed.*, 2007, **46**, 3750-3753.

37 T. Yamagata, J. Kuwabara and T. Kanbara, *Tetrahedron*, 2014, **70**, 1451-1457.

38 X.-Y. Zhu, H.-W. Yao, Y.-J. Fu, X.-F. Guo and H. Wang, *Anal. Chim. Acta*, 2019, **1048**, 194-203.

39 M. Pieczykolan, B. Sadowski and D. T. Gryko, *Angew. Chem. Int. Ed.*, 2020, ahead of press.

40 A. J. Stasyuk, P. J. Cywiński and D. T. Gryko, *J. Photochem. Photobiol. C*, 2016, **28**, 116-137.

41 D. Firmansyah, I. Deperasińska, O. Vakuliuk, M. Banasiewicz, M. Tasior, A. Makarewicz, M. K. Cyrański, B. Kozankiewicz and D. T. Gryko, *Chem. Commun.*, 2016, **52**, 1262-1265.

42 A. J. Stasyuk, M. Banasiewicz, M. K. Cyrański and D. T. Gryko, *J. Org. Chem.*, 2012, **77**, 5552-5558.

43 S. H. Reich, P. A. Sprengeler, G. G. Chiang, J. R. Appleman, J. Chen, J. Clarine, B. Eam, J. T. Ernst, Q. Han, V. K. Goel, E. Z. R. Han, V. Huang, I. N. J. Hung, A. Jemison, K. A. Jessen, J. Molter, D. Murphy, M. Neal, G. S. Parker, M. Shaghafi, S. Sperry, J. Staunton, C. R. Stumpf, P. A. Thompson, C. Tran, S. E. Webber, C. J. Wegerski, H. Zheng and K. R. Webster, *J. Med. Chem.*, 2018, **61**, 3516-3540.

44 N. D. Kushwaha, S. Mondal, R. Sharma and N. Kumar, *Asian J. Chem.*, 2017, **29**, 1495-1498.

45 B. S. Rane, M. A. Kazi, S. M. Bagul, D. P. Shelar, R. B. Toche and M. N. Jachak, *J. Fluoresc.*, 2010, **20**, 415-420.

46 N. Perin, J. Alić, S. Liekens, A. Van Aerschot, P. Vervaeke, B. Gadakh and M. Hranjec, *New J. Chem.*, 2018, **42**, 7096-7104.

47 Z.-B. Sun, M. Guo and C.-H. Zhao, *J. Org. Chem.*, 2016, **81**, 229-237.

48 E. N. Nuraneeva, G. B. Guseva, E. V. Antina, R. T. Kuznetsova, M. B. Berezin and A. I. V'yugin, *Russ. J. Gen. Chem.*, 2016, **86**, 840-847.

49 A. Matsumoto, R. Nishiyabu and Y. Kubo, *RSC Adv.*, 2014, **4**, 37973-37978.

50 E. Marchal, D. A. Smithen, M. I. Uddin, A. W. Robertson, D. L. Jakeman, V. Mollard, C. D. Goodman, K. S. MacDougall, S. A. McFarland, G. I. McFadden and A. Thompson, *Org. Biomol. Chem.*, 2014, **12**, 4132-4142.

51 S. Shimizu, *Chem. Commun.*, 2019, **55**, 8722-8743.

52 P. B. Thale, P. N. Borase and G. S. Shankarling, *Dalton Trans.*, 2015, **44**, 13947-13954.

53 X. Wang, H.-t. Liu, J. Cui, Y. Wu, H. Lu, J. Lu, Z. Liu and W. He, *New J. Chem.*, 2014, **38**, 1277-1283.

54 Y. Zhou, Y. Xiao, D. Li, M. Fu and X. Qian, *J. Org. Chem.*, 2008, **73**, 1571-1574.

55 T. Lundrigan, A. E. G. Baker, L. E. Longobardi, T. E. Wood, D. A. Smithen, S. M. Crawford, T. S. Cameron and A. Thompson, *Org. Lett.*, 2012, **14**, 2158-2161.

56 A. S. Murphy, C. E. Killalea, J. Humphreys, P. A. Hume, M. J. Cliffe, G. J. Murray, E. S. Davies, W. Lewis and D. B. Amabilino, *ChemPlusChem*, 2019, **84**, 1413-1422.

57 R. A. Marcus, *J. Phys. Chem.*, 1989, **93**, 3078-3086.

58 J. Cortes, H. Heitele and J. Jortner, *J. Phys. Chem.*, 1994, **98**, 2527-2536.

59 I. R. Gould, R. H. Young, R. E. Moody and S. Farid, *J. Phys. Chem.*, 1991, **95**, 2068-2080.

60 J. Herbich and A. Kapturkiewicz, *J. Am. Chem. Soc.*, 1998, **120**, 1014-1029.

61 D. Jacquemin, A. Planchat, C. Adamo and B. Mennucci, *J. Chem. Theory Comput.*, 2012, **8**, 2359-2372.

62 F. Santoro and D. Jacquemin, *WIREs Comput. Mol. Sci.*, 2016, **6**, 460-486.

63 I. Ciofini, T. Le Bahers, C. Adamo, F. Odobel and D. Jacquemin, *J. Phys. Chem. C*, 2012, **116**, 11946-11955.

64 T. Le Bahers, C. Adamo and I. Ciofini, *J. Chem. Theory Comput.*, 2011, **7**, 2498-2506.

Table of contents graphic

DPP-BODIPY hybrids have been synthesized for the first time using unsymmetrical, imidazo[1,2-*a*]pyridine substituted DPPs which display increased photostability and bathochromically shifted absorption and fluorescence.